ADVANCED MATERIALS

[7] M. Böltau, S. Walheim, J. Mlynek, G. Krausch, U. Steiner, *Nature* **1998**, *391*, 877.
[8] S. Y. Chou, L. Zhuang, L. Guo, *Appl. Phys. Lett.* **1999**, *75*, 1004.
[9] E. Schäffer, T. Thurn-Albrecht, T. P. Russell, U. Steiner, *Nature* **2000**, *403*, 874.
[10] E. Schäffer, S. Harkema, R. Blossey, U. Steiner, *Europhys. Lett.* **2002**, *60*, 255.
[11] A. Karim, J. F. Douglas, B. P. Lee, J. A. Rogers, R. J. Jackman, E. J. Amis, G. M. Whitesides, *Phys. Rev. E* **1998**, *57*, 273.
[12] S. Walheim, M. Ramstein, U. Steiner, *Langmuir* **1999**, *15*, 4828.
[13] R. Sherman, D. Hirt, R. J. Vane, *J. Vac. Sci. Technol.* **1994**, *12*, 1876.
[14] Y. Xia, J. Tien, D. Qin, G. Whitesides, *Langmuir* **1996**, *12*, 4033.
[15] C. Bechinger, H. Muffler, C. Schäfle, O. Sundberg, P. Leiderer, *Thin Solid Films* **2000**, *366*, 135.
[16] F. Burmeister, C. Schäfle, B. Keilhofer, C. Bechinger, J. Boneberg, P. Leiderer, *Adv. Mater.* **1998**, *10*, 495.
[17] M. Sprenger, S. Walheim, A. Budkowski, U. Steiner, *Interface Sci.* **2003**, *11*, 225.
[18] K. Fukunaga, H. Elbs, G. Krausch, *Langmuir* **2000**, *16*, 3474.

Palladium Nanotubes with Tailored Wall Morphologies

By *Martin Steinhart*, *Zhihong Jia*, *Andreas K. Schaper*, *Ralf B. Wehrspohn*,* *Ulrich Gösele*, and *Joachim H. Wendorff*

Nanotubes have an outstanding potential to transport or store gases and fluids for fuel cells, energy conversion, catalysis, and drug release.[1–10] Nanotube walls with an internal fine structure and thus a high specific interface area should strongly enhance the reactivity as well as the capability for adsorption. Furthermore, the efficiency of transport processes within and across the nanotube walls should be improved. We report on a simple method to generate nanotubes with controllable wall morphology or porosity in the nanometer range. It consists of three steps: the formation of multi-component nanotubes; demixing to generate coexisting phases within the tube walls; and the controlled ripening of the phase morphology. Depending on the selected components, their concentrations, and the ripening stage, nanotubes with characteristic wall morphologies were obtained. Selective removal of one component yields residual nanotubes with a specific nanoroughness and a controllable porosity. This fundamental concept should be applicable to a broad range of materials. We will demonstrate this exemplarily by means of structured palladium nanotubes, since palladium nanoparticles are of considerable interest for catalysis,[11–14] sensor technology,[15] and hydrogen storage.[16]

Decomposition in thin films on smooth substrates has been investigated extensively.[17] Spinodal demixing induced either by a thermal quench or by the evaporation of a solvent generates a co-continuous phase morphology with a characteristic length. Simultaneously, ripening occurs to reduce the initially large internal interface area. The phase morphology is strongly affected by substrate/film and film/air interfaces, as well as by confinement effects.[18–22] Several groups have used thin films structured by phase separation for devices such as transistors,[23] light emitting diodes,[24] or photodiodes.[25] It would be advantageous if nanotubes with such well-defined morphologies could be obtained in a controlled way. However, to date, the range of wall morphologies accessible by preparation methods such as self-assembly[1–5] and the use of templates[6–10] is limited to core–shell structures via consecutive synthetic steps.[6,10] Our approach is based on wetting porous matrices that exhibit high surface energies with multicomponent melts or solutions containing polymers.[26] A mesoscopic film of the wetting liquid covers the pore walls rapidly, since polymers adsorb avidly on high energy surfaces.[27] A kinetically stable stationary state is generated when all adsorption sites on the pore wall are occupied. Solidification of the wetting liquid at this stage results in the preservation of nanotubes. Decomposition can be induced by solvent evaporation during wetting or by thermal quenching. Ripening occurs after the onset of phase separation, as long as the solvent concentration is sufficiently high to prevent solidification, or if the system is annealed at temperatures where at least one component is liquid. Freezing of the ripening process can be achieved by cooling below the glass temperature of a polymeric component, by the onset of crystallization, by crosslinking, or by the selective removal of one component. Wall morphologies ranging from a molecular-disperse distribution of the components to co-continuous networks or matrix-dispersed particles should be accessible.

To prepare palladium nanotubes, we wetted ordered, porous alumina[28] with solutions containing poly(D,L-lactide) (PDLLA) and palladium(II) acetate ($Pd(OAc)_2$) in a ratio of 1:1, under ambient conditions. Solid PDLLA/$Pd(OAc)_2$ nanotubes were obtained after the solvent (dichloromethane or chloroform) was evaporated. Phase separation took place when the solvent concentration fell below a certain threshold. Annealing at 200 °C led to the thermal degradation of $Pd(OAc)_2$ within a few tens of seconds and Pd^{II} was reduced to Pd^0. The formation of polycrystalline face-centered cubic (fcc) palladium was confirmed by selected-area electron diffraction (SAED). Figure 1a shows a transmission electron microscopy (TEM) image of an ultrathin section of porous alumina (pore diameter $D_p = 55$ nm, pore depth $t_p = 50$ μm) after wetting and annealing for 5 min at 200 °C. The pore walls are covered by a PDLLA/Pd layer with a thickness of about 10 nm that does not exhibit a pronounced internal morphology. Some palladium nanoparticles, a few nanometers in size,

[*] Prof. R. B. Wehrspohn, M. Steinhart, Prof. U. Gösele
Max-Planck-Institute of Microstructure Physics
Weinberg 2, D-06120 Halle (Germany)
email: wehrspoh@mpi-halle.de
M. Steinhart, Prof. J. H. Wendorff
Institute of Physical Chemistry, Philipps-Universtity
Hans-Meerwein Strasse, D-35032 Marburg (Germany)
Z. Jia, Dr. A. K. Schaper, Prof. J. H. Wendorff
Center of Material Science, Philipps-Universtity
Hans-Meerwein Strasse, D-35032 Marburg (Germany)

[**] Support from the Deutsche Forschungsgemeinschaft (WE 2637/1-1 and WE 496/19-1) and the donation of polylactides form Böhringer Ingelheim are gratefully acknowledged. We thank Petra Göring, Jinsub Choi, Kornelius Nielsch, Katrin Schwirn, Stefan Schweizer, Jörg Schilling, and Sven Matthias for the preparation of the templates, as well as Dr. H. Hofmeister for additional TEM investigations.

  DOI: 10.1002/adma.200304502

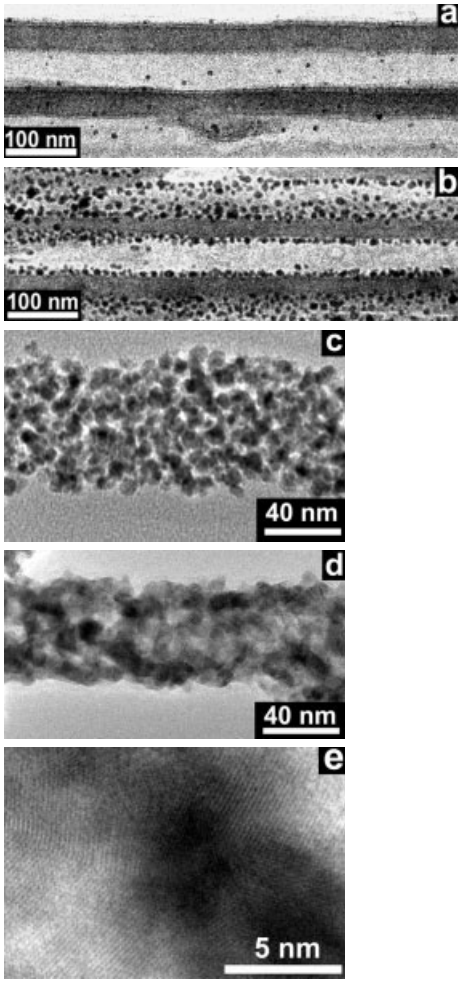

Fig. 1. TEM images of PDLLA/Pd and Pd nanotubes obtained by wetting porous alumina: $D_p = 55$ nm (except (c), where $D_p = 70$ nm) and $t_p = 50$ μm. a) Ultrathin section of a wetted template after annealing for 5 min at 200 °C. The alumina pore walls are covered with thin PDLLA/Pd layers that look like stained polymer films. b) The same sample, but annealed for 24 h at 200 °C. The tube walls covering the pore walls contain a monolayer of palladium nanoparticles. c) Pd nanotube, prepared by annealing of PDLLA/Pd composite tubes within the template for 24 h, after removing PDLLA and the template. d) Pd nanotube, prepared by annealing PDLLA/Pd composite tubes within the template for 48 h, after removing PDLLA and the template. e) High-resolution TEM image showing details of the wall of the Pd nanotube shown in Figure 2d.

are visible, but the majority of palladium atoms are still dispersed within the tube walls, corresponding to an early ripening stage. No tubular palladium structures were preserved after removing the PDLLA and the template. Annealing the sample for 24 h at 200 °C, resulted in tube walls containing a monolayer of palladium particles ranging in size from 5 to 10 nm (Fig. 1b). They form a network that is stable even without support (Fig. 1c). With increasing ripening time, the wall morphology became significantly coarser. After 48 h annealing, the palladium crystallites extended 20–50 nm (Fig. 1d). The residual palladium nanotubes have a length of several micrometers. The tube walls exhibit a polycrystalline nature, as determined by high-resolution TEM investigations (Fig. 1e).

The shape of the template pores not only determines the shape of the nanotubes, but it also affects their internal morphology. We expected two effects if D_p and t_p were increased to 400 nm and 100 μm, respectively. Firstly, the curvature of the nanotube walls should reduce the growth rate of the palladium nanocrystallites. In a thin film without curvature, the crystal facets exhibiting the highest growth rate will be oriented normal to the film plane to maximize the growth rate in the directions where the system is infinite. However, in a curved geometry, they are displaced if the crystallites adopt the curvature. Crystal facets with a lower growth rate must thus contribute to the growth process too. This effect should be less pronounced if the curvature is reduced by increasing D_p. Actually, the growth rate was significantly higher for $D_p = 400$ nm than for $D_p = 55$ nm. Walls containing interconnected palladium crystallites extending 20–50 nm were already obtained by annealing for 6 h at 200 °C (Fig. 2a). The removal of PDLLA and the template yields residual palladium nanotubes with lengths of some tens of micrometers (Fig. 2b) and wall thicknesses of about 10 nm (Fig. 2c).

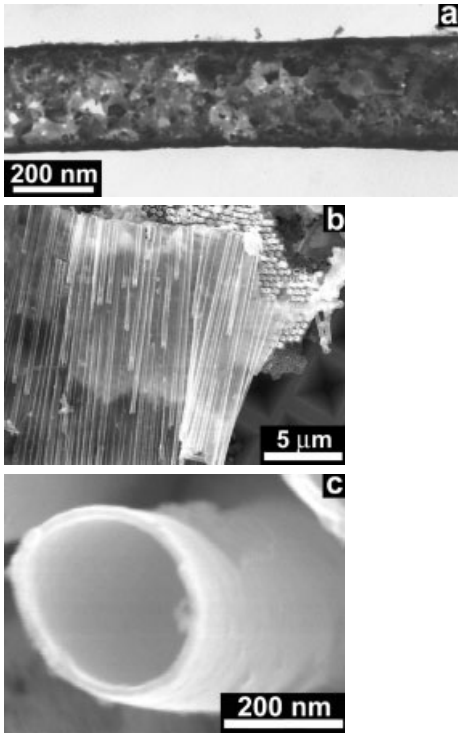

Fig. 2. Pd nanotubes obtained by wetting porous alumina, $D_p = 400$ nm and $t_p = 100$ μm, after annealing for 6 h at 200 °C and removing PDLLA and the template. a) TEM image of an individual palladium nanotube showing wall detail. b) Scanning electron microscopy (SEM) image of an array of aligned palladium nanotubes. c) SEM image of a cross-section of an individual nanotube.

Secondly, the initial morphology of the nanotubes prior to annealing was affected by the pore depth. The solvent was first depleted at the pore bottom, and subsequently at the pore opening, since the pores of all the alumina templates used here were blind holes. The ripening period becomes longer with decreasing distance from the pore opening. Increasing t_p from 50 to 100 μm extended the ripening period for the nanotube segments adjacent to the pore opening such that their walls contained interconnected palladium crystal-

ADVANCED MATERIALS

lites with a broad size distribution after solidification and reduction of Pd^{II}. They have no direct contact with the pore wall, indicating the existence of a PDLLA wetting layer on the alumina surface (Fig. 3a). This is consistent with the fact that inorganic materials such as palladium exhibit much higher surface energies than organic polymers.[29] The interconnected palladium crystallites formed stable tubular structures with lengths of approximately 4 μm without support, whereas the crystallite size decreased and the tubular structure collapsed at larger distances from the pore opening (Fig. 3b). Ripening gradients within individual nanotubes thus occur if t_p is sufficiently large.

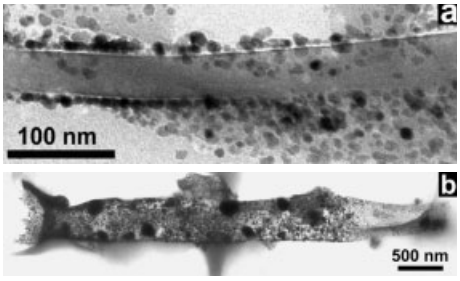

Fig. 3. Initial morphologies of PDLLA/Pd and the residual Pd nanotubes generated by solvent evaporation after wetting the porous alumina: $D_p = 400$ nm and $t_p = 100$ μm. a) TEM image of an ultrathin section of a template wetted with a PDLLA/Pd layer. The area shown here was in the vicinity of the pore opening. There is no direct contact between the palladium particles and the alumina pore wall, indicating the existence of a PDLLA wetting layer. b) TEM image of a Pd nanotube segment (after removing PDLLA and the template) that was in the vicinity of the template pore's opening. The tube opening on the left was located at the pore opening.

The morphologies of the nanotubes were generated by spinodal decomposition and controlled ripening. If PDLLA was in the liquid state, palladium atoms diffused avidly, whereas below its glass transition temperature the structure formation was frozen. This was confirmed by an analysis of the morphologies of PDLLA/Pd composite films (thickness 250 nm) that were annealed at 200 °C, for 0, 6, and 24 h. We took Fourier transforms of scanning electron micrographs of the residual palladium films after removing PDLLA, and obtained pronounced halos. A short-range order that is typical for a spinodal demixing was initially generated by the decomposition of the PDLLA/$Pd(OAc)_2$ solution used for spin-coating, and this was preserved after reducing the palladium. Statistical analysis of the film morphologies provided characteristic distributions of the spinodal wavelengths. With increasing annealing time, the morphology of the films coarsened significantly. The most frequent wavelength was initially of the order of 60 nm (Fig. 4a). After 6 and 24 h, the most frequent spinodal wavelength increased to approximately 130 and 230 nm, respectively (Fig. 4b).

We have demonstrated that the controlled adjustment of the parameters that determine demixing and ripening provides nanotubes with tailored wall morphologies. As an example, we adjusted the size of palladium domains in PDLLA/Pd nanotubes, ranging from a molecular-dispersed distribution to a continuous network of anisotropic nanocrystallites.

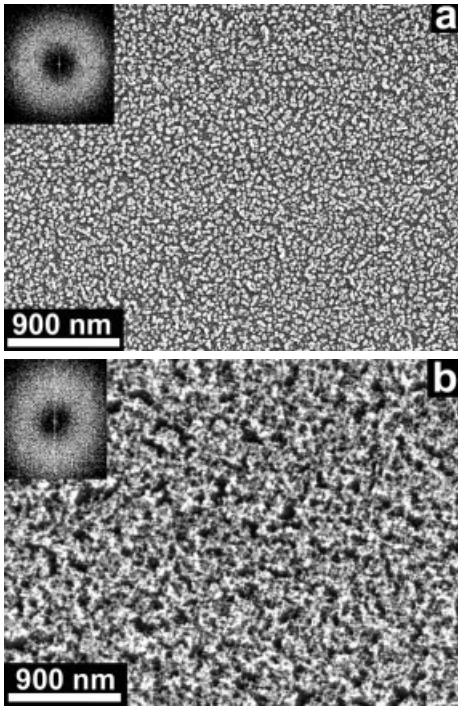

Fig. 4. Morphologies of PDLLA/Pd composite films (thickness 250 nm) prepared by spin-coating a PDLLA/$Pd(OAc)_2$ solution. The SEM images show residual palladium films annealed for a) 0 and b) 24 h at 200 °C prior to the removal of PDLLA. The corresponding halos (insets) were obtained by taking Fourier transforms of the micrographs (normalized to the correlation length).

Experimental

We used palladium(II) acetate purchased from Aldrich (cat. no. 20 5869) and PDLLA Resomer R 208 from Böhringer Ingelheim. 1.2 to 2.5 wt.-% of 1:1 mixtures of both compounds were dissolved in freshly distilled CH_2Cl_2 or $CHCl_3$. The dark red solutions were dropped onto the templates using a syringe, under ambient conditions. To remove PDLLA from the composite tubes selectively by pyrolysis, the samples were annealed for 90 min in a vacuum at 350 °C. To remove the template selectively, it was immersed into 40 wt.-% aqueous KOH at room temperature. The palladium tubes were obtained as a black powder, which was washed with water and ethanol several times to remove the KOH. For all SEM experiments, a JEOL JSM 6300F scanning electron microscope was used. To prepare the nanotubes as a powder, the samples were suspended in ethanol by applying ultrasound. Then, the suspension was dropped onto conductive substrates, such as silicon wafers. For the TEM investigations, we dropped the suspensions onto copper grids coated with a thin carbon film. We used a JEM 3010 TEM operating at an accelerating voltage of 300 kV.

Received: October 9, 2002
Final version: January 20, 2003

[1] G. M. Whitesides, J. P. Mathias, C. T. Seto, *Science* **1991**, *254*, 1312.
[2] G. A. Ozin, *Adv. Mater.* **1992**, *4*, 612.
[3] J. M. Schnur, *Science* **1993**, *262*, 1669.
[4] M. Ghadiri, J. R. Granja, L. K. Buehler, *Nature* **1994**, *369*, 301.
[5] S. Iijima, *Nature* **1991**, *354*, 56.
[6] M. Bognitzki, H. Hou, M. Ishaque, T. Frese, M. Hellwig, C. Schwarte, A. Schaper, J. H. Wendorff, A. Greiner, *Adv. Mater.* **2000**, *12*, 637.
[7] K. S. Mayya, D. I. Gittins, A. M. Dibaj, F. Caruso, *Nano Lett.* **2001**, *1*, 727.
[8] C. R. Martin, *Science* **1994**, *266*, 1961.
[9] E. Evans, H. Brownman, A. Leung, D. Needham, D. Tirrell, *Science* **1996**, *273*, 933.
[10] J. C. Hulteen, C. R. Martin, *J. Mater. Chem.* **1997**, *7*, 1075.
[11] S. Niwa, M. Eswarmoorthy, J. Nair, A. Raj, N. Itoh, H. Shoji, T. Namba, F. Mizukami, *Science* **2002**, *295*, 105.

[12] C. P. Mehnert, D. W. Weaver, J. Y. Ying, *J. Am. Chem. Soc.* **1998**, *120*, 12 289.
[13] Y. Li, X. M. Hong, D. M. Collard, M. A. El-Sayed, *Org. Lett.* **2000**, *2*, 2385.
[14] S.-W. Kim, M. Kim, W. Y. Lee, T. Hyeon, *J. Am. Chem. Soc.* **2002**, *124*, 7642.
[15] F. Favier, E. C. Walter, M. P. Zach, T. Benter, R. M. Penner, *Science* **2001**, *293*, 2227.
[16] *Hydrogen in Metals III* (Ed: H. Wipf), Springer, Berlin **1997**.
[17] T. Hashimoto, *Structure and Properties of Polymers*, Materials Science and Technology, Vol. 12, VCH, Weinheim **1993**.
[18] K. Binder, *J. Non-Equilib. Thermodyn.* **1998**, *23*, 1.
[19] J. W. Cahn, *J. Chem. Phys.* **1977**, *66*, 3667.
[20] R. A. L. Jones, L. J. Norton, E. J. Kramer, F. S. Bates, P. Wiltzius, *Phys. Rev. Lett.* **1991**, *66*, 1326.
[21] G. Krausch, C.-A. Dai, E. J. Kramer, F. S. Bates, *Ber. Bunsenges. Phys. Chem.* **1994**, *98*, 446.
[22] L. Sung, A. Karim, J. F. Douglas, C. C. Han, *Phys. Rev. Lett.* **1996**, *76*, 4368.
[23] Y. Yang, A. J. Heeger, *Nature* **1994**, *372*, 344.
[24] M. Berggren, O. Inganas, G. Gustaffson, J. Ramusson, M. R. Andersson, T. Hjertberg, O. Wennerstöm, *Nature* **1994**, *373*, 444.
[25] J. J. M. Halls, C. A. Walsh, N. C. Greenham, E. A. Marseglia, R. H. Friend, S. C. Moratti, A. B. Holmes, *Nature* **1995**, *376*, 498.
[26] M. Steinhart, J. H. Wendorff, A. Greiner, R. B. Wehrspohn, K. Nielsch, J. Schilling, J. Choi, U. Gösele, *Science* **2002**, *296*, 1997.
[27] J. N. Israelachvili, *Intermolecular and Surface Forces*, 2nd ed., Academic Press, London **1991**, pp. 291–294.
[28] H. Masuda, K. Fukuda, *Science* **1995**, *268*, 1466.
[29] S. Wu, *Polymer Interface and Adhesion*, Dekker, New York **1982**.

Selected Polymorphs of $CaCO_3$ Through Epitaxy with Inorganic Substrates Aligned with an Electric Field**

By *Il Won Kim*, *Richard E. Robertson*,* and *Robert Zand*

Mineral-containing biological materials have attracted great interest because their well-defined structures produce exceptionally intriguing optical, magnetic, and mechanical properties. Such optical properties are illustrated in a photoresponsive species by the coordinated crystals of calcite. The crystals form microlenses that guide and focus light on nerve bundles.[1]

Fascinating magnetic properties are represented in magnetotactic bacteria by iron-rich magnetic crystals. The crystals constitute magnetosomes that enable alignment and navigation along the Earth's geomagnetic field lines.[2] Superior mechanical properties are exemplified in mollusks by the highly organized crystals of aragonite. The crystals assemble in nacreous layers that show remarkable toughness, 3000 times more than that of geological aragonite, even with a very high content of brittle inorganic crystals (ca. 99 %).[3,4] These phenomena are closely related to the orientation and polymorphism of the mineral crystals, which are controlled by nucleation.[2,3,5,6] The control of orientation by nucleation is relatively well established. Monolayer studies show one-dimensional orientation induced by stereochemical match between substrate and growing crystals.[5–7] The degree of orientation increases with epitaxy.[8] In contrast, the control of polymorphism by nucleation is not well understood, and aragonite formation among the three $CaCO_3$ polymorphs (aragonite, calcite, and vaterite) has been especially elusive. Aragonite is thermodynamically less stable than calcite, and its formation in biological materials is made under kinetically unfavorable conditions.[3] To elucidate the mechanism of this perplexing phenomenon, several in vitro studies have been attempted with limited success. Aragonite formation is demonstrated with macromolecules extracted from the nacre of mollusks, but the selection mechanism is unclear because of the complexity of the system.[9] Monolayer studies suggest the importance of geometric correspondence, but the lack of exclusive aragonite formation and the difficulty of systematic studies make the analysis of these systems inconclusive.[10,11]

In the present study, aragonite was grown under calcite-favorable conditions on aragonite-type inorganic substrates that could be oriented by aligning them in a polymer resin by an electric field. The lattice parameters of the substrates were systematically varied to study the effect of epitaxial strain on polymorphism. The critical epitaxial strain for aragonite to grow was found to be in the range 5–7 %.

The inorganic crystal substrates used in the present study were $SrCO_3$, $PbCO_3$, and $BaCO_3$. These have the same orthorhombic *Pnma* structure as aragonite. The lattice parameters of the crystals expand as the size of cations increases: $CaCO_3$ < $SrCO_3$ < $PbCO_3$ < $BaCO_3$.[12] The crystals were synthesized by heating aqueous solutions of $SrCl_2$, $PbCl_2$, or $BaCl_2$ and urea.[13] Needle-shaped $SrCO_3$ and $BaCO_3$ crystals with aspect ratios in the range 10–20 were collected. $PbCO_3$ crystals initially formed as thin plates, though later they formed mainly as elongated needles.

The crystallographic orientations of the carbonate crystals were identified by two methods: X-ray diffraction (XRD) in the 2θ–θ mode and morphological analysis. First, XRD samples were prepared by mechanically shearing the crystals in vacuum grease to align the long axes of the crystals parallel to the X-ray stage. Since the (00*l*) peaks disappeared and the (*hk*0) peaks were intensified compared to those for randomly oriented crystals, the long axes were determined to be parallel to the *c*-axis.[7,14] The (002) peak of $PbCO_3$ did not completely disappear because of the presence of the thin plates. The long axis of the platelet crystals is within the *ab*-plane as explained in the following morphological analysis.

Crystal morphology was observed with scanning electron microscopy (SEM) after Au/Pd coating. $SrCO_3$ and $BaCO_3$ needles have similar pseudo-hexagonal cross sections, which are common for twins of aragonite-type crystals.[15] The char-

[*] Prof. R. E. Robertson, I. W. Kim
Macromolecular Science & Engineering Center and
Department of Materials Science & Engineering
The University of Michigan
Ann Arbor, MI 48109-2136 (USA)
E-mail: rer@umich.edu
Prof. R. Zand
Macromolecular Science & Engineering Center,
Biophysics Research Division, and
Department of Biological Chemistry
The University of Michigan
Ann Arbor, MI 48109-1055 (USA)

[**] We thank Dr. J. Aizenberg, Prof. A. J. Matzger, and Mr. K. Kim for useful discussions, and Mr. D. Jang for his help with the XRD experiment.

 DOI: 10.1002/adma.200304413